Negative Results on Deploying Distributed Series Reactance Devices to Improve Power System Robustness Against Cascading Failures

Arash Beiranvand, *Student Member, IEEE* and Paul Cuffe, *Member, IEEE*

***Abstract*—Distributed Series Reactances are devices that dynamically increase the impedance of a line to reduce the power flow it carries. This work explores whether widely deploying these devices enhances a power system's robustness against line overload cascading failures. The presence of Distributed Series Reactances may make it less likely that equipped lines would become overloaded by contingencies elsewhere, and so their presence may arrest the propagation of line overloads through a system. However, the efficacy of these devices in this role has not been widely investigated. Likewise, there are few extant methodologies for siting dynamic reactances within the grid to mitigate the propagation of cascades. In this paper, the ability of these devices to arrest the propagation of cascading failures within power grids is investigated. First, a novel DC power flow is formulated, which models dynamic line impedances. A novel methodology is proposed for siting the devices on lines spread throughout the network. With these innovations in hand, the devices' effects on cascade propagation are simulated using a sizeable database consisting of multiple load & generation snapshots across eight test networks. No major beneficial effect is found, even when 25% of lines are equipped.**

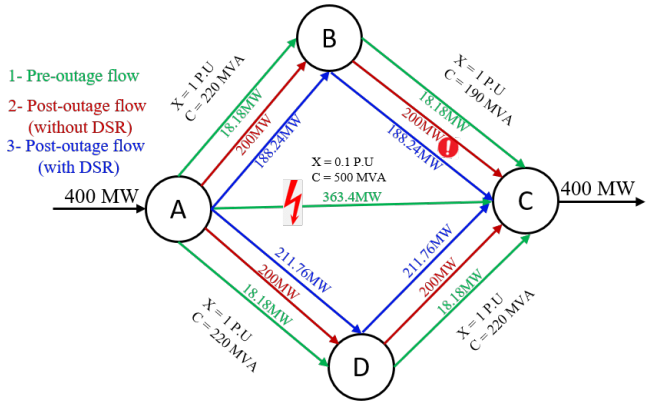

Fig. 1. An example power transaction from node A to C: in the **post-outage without applying DSR** situation, the power divides evenly between the upper and lower paths. This power redistribution puts the loading along $B \rightarrow C$ beyond its thermal capacity

I. Introduction

Power electronics devices can enhance the resiliency of power systems [1]. Intuitively, a Flexible AC Transmission System (FACTS) device with the ability to reduce power flow within a particular line may be able to arrest the broader propagation of cascading overload outages as well. This seems initially plausible, as a sufficient reduction in the power flow of an overloaded line by a FACTS device stops it tripping off during the cascade's propagation.

Power flow within a line can be controlled by altering the series line impedance, voltage bus magnitude, or the voltage angles of buses [2]. Several FACTS devices have been designed to change these factors to control the power flow in a line such as series reactors, static series synchronous compensator, etc [2]. Among the devices with the ability to change power flows, Distributed Series Reactances (DSR) are one of the most installed types within grids. The reasons for this increasing tendency to install more DSR devices within the grids include but are not limited to: their ability to reduce power flows within the lines, low-cost operation, fast installation, and their simple structures [2].

In modern power grids, various applications are considered for DSR, including but not limited to: power system reliability improvement, reduction of congestion, increasing the loadability of the grid, phase balancing, etc [2], [3]. The authors in [4] suggest using DSR modules to improve voltage imbalance within power grids and argue the proposed methodology benefits dynamic flexibility to cope with various sources of the imbalance. [5] applies DSR devices to eliminate the lines' congestion and consequently, decrease the related costs in power market. In [6], the economic advantages of applying DSR within the grids due to the lines' congestion relief are investigated. Also, a novel metric is proposed to measure the loading capacity increase due to applying the DSR units for the transmission network. In [7], the capability of implementing smart wires like DSR to handle the operational problems due to adopting the grids with new environmental policies is investigated.

Moreover, some few studies have considered the effects of DSR on the reliability analysis of power grids. For example, in [8], a planning study for a specific power grid integrated with renewable energy sources is presented that, as one of its goals, aims to minimise the amount of load-shedding in the presence of DSR modules. In [9], considering $N-1$ contingencies constraints, the planning problem of a transmission system with continuously variable series reactors is modeled. Considering

A. Beiranvand (arash.beiranvand@ucdconnect.ie) and P. Cuffe are with the School of Electrical and Electronic Engineering, University College Dublin. This publication has emanated from research supported in part by Science Foundation Ireland (SFI) under the SFI Strategic Partnership Programme Grant Number SFI/15/SPP/E3125 and additional funding provided by the UCD Energy Institute. The opinions, findings and conclusions or recommendations expressed in this material are those of the authors and do not necessarily reflect the views of the Science Foundation Ireland.

a set of contingencies, in [10] a probabilistic transmission planning problem in the presence of DSR devices is formulated.

Power grids are prone to cascading line outages because they can be quite 'brittle' at some specific load-generation profiles, termed as transition points [11], [12], whereby small contingencies are sufficient to trigger a long subsequent chain of cascades which could result in a collapse of the entire system [12]. At the transition points, the damage' size, in terms of the load-shedding, caused by the cascades significantly increases in comparison with it for the other load-generation profiles of the grid [11], [12]. Several previous studies in the literature have investigated these transition points [11]–[14]. In [14] it is argued the topology of the grid is also capable of altering its transition points. Power systems may be operated near these transition points [12] where the risk of widespread cascading outages starts to rise rapidly [11]. At the transition points, even small contingencies can rapidly, and sometimes non-locally [15], propagate across the network so that the grid may not be able to tolerate the outages and consequently, experiences severe damages. The non-linear relationship between the size of the triggering outages and the size of the resulted blackout is due to the strong interactions between many available components within the gird, especially at the transition points [14]. These important insights are suggestive of the brittleness of the girds against some contingencies that could lead to catastrophic cascading outages.

Cascading line outages are progressive events whereby tripping one overloaded line transfers its power flow to other lines, putting them over their thermal limits, in turn, causing further tripping and adverse redistribution of power flow [16]. This progressive rapid overloading across the network can lead to widespread outages and significant load-shedding throughout the grid. Thus, mitigating cascading line outages has always been a major concern for power system robustness. Various online mitigation strategies can be considered by the control room. For instance, in [17] a load-shedding based strategy is proposed to mitigate the cascading outages. In [18], readjusting the resources and changing the grid's topology are considered for the mitigation strategy. Using a dynamic interaction graph, the proposed mitigation strategy in [19] finds the most critical lines within the grids in terms of the cascading outages and then applies a specific optimal power flow to prevent tripping of the detected lines. [20] proposes a framework to mitigate cascading outages through optimizing the available control within the transmission grid.

The power flow equations imply that if we increase a line's impedance, its loading will typically decrease, depending on how much the impedance increases and what alternative paths are available within the grid for the line's flow. Thus, decreasing the loading of overloaded lines by dynamically increasing their impedance seems a reasonable measure to keep such lines online and consequently, arrest the propagation of cascades. DSR are capable of increasing the lines' impedance and therefore, can serve this purpose so that the device can help the grids handle the redistributed active power of the outaged lines and prevent the systems to badly react to the subsequent outages. These important facts suggest the intuition of applying the modules to make the grid less brittle against the cascades can be quite legitimate. Hence, the present paper investigates these important research questions: Can we arrest cascading line outages by applying DSR modules to dynamically modulate lines' impedance and thereby decrease their loading? Can widespread deployment of DSRs make the grids less brittle in the face of cascading failure?

Intuitively, DSR modules seem to be capable of arresting the cascades' propagation. Consider the sample power grid presented in Fig. 1. In the normal operation, all lines are working in their permitted loading thresholds for a 400 MW power transaction between A and C. If line $A \rightarrow C$ is tripped off due to a failure, its pre-outage flow will be equally redistributed to the paths $A \rightarrow B \rightarrow C$ and $A \rightarrow D \rightarrow C$ which results in 200 MW loading for each line. However, 200 MW is beyond the loading capacity of line $B \rightarrow C$ and consequently, this line will be tripped off too. In such a condition, the only available path for 400 MW transaction between nodes A and C is $A \rightarrow D \rightarrow C$. This means that $A \rightarrow D$ and $D \rightarrow C$ will be loaded to 400 MW and consequently, these two lines will be tripped off as well and the connection between A and C will be severed. Now, assume that line $B \rightarrow C$ is equipped with sufficient DSR modules to automatically increase the line impedance by 25% when the line is heavily loaded. In such circumstances, after the $A \rightarrow C$ outage, the DSR units in line $B \rightarrow C$ will increase the line impedance to 1.25 p.u. This increase of the line impedance reduces the flow through line $B \rightarrow C$ and redistributes it onto the path $A \rightarrow D \rightarrow C$. Due to this redistribution, the lines within the paths $A \rightarrow B \rightarrow C$ and $A \rightarrow D \rightarrow C$ will be loaded by 188.24 MW and 211.76 MW, respectively, which fall in the thermal capacities of the corresponding lines. This means no further outages occur and the grid is saved by the DSR modules. This significant intuition alongside the practical advantages of modules like their low operations costs, simple structures and, easy installations suggest that DSRs could be affordable and effective devices to mitigate the cascades.

Despite the clear abilities of DSR to prevent an individual line being tripped off due to overloading, there is little research on how the presence of DSR units may affect the sequence of progressive line overload tripping in transmission systems following a contingency. No clear insight is available regarding the devices' general effects on cascade propagation. For example, do the devices tend to arrest the propagation of line outage cascades? How can they be located within grids to have the best opportunity to mitigate cascades? The present paper addresses this gap in the literature and aims to investigate if DSR devices can have a new role as controlling facilities against the cascading line outages in addition to their usual applications.

To analyse the cascading line outages, this paper adapts an established simulation procedure [21] which at each step of the cascade removes the overloaded lines and in any resulting islands maintains balance between generation and demand. A major novel challenge is that at each step of the cascading failures we need to solve DC power flow in the presence of dynamic impedances to model the effect of DSR on the next steps of the cascades.

By introducing a mutual dependence between a line's total reactance and the power flow through it, these devices add non-linearity to the power flow calculations [2], [3]. The DC load flow equations in the presence of the dynamic impedances have a Quadratic Constraint Programming (QCP) configuration [3].

In general, QCP problems can be converted to Mixed Integer Linear Programming (MILP) problems by *spatial branching* [22]. Such formulation entails auxiliary binary variables that increase the problem complexity. The solution accuracy depends on the number of binary variables and the performance of the branching approach. For example, in [3], an approximate MILP formulation based on spatial branching was proposed and also used in [23] to minimize the system operation cost in the presence of variable impedances. The solution accuracy was validated in the case studies. However, the solution time might not suit the quasi-real-time applications as mentioned in [3], [23] and therefore further approximations are considered to deal with this complexity. The same efforts to model dynamic impedance have been carried out in [24] so that the original non-linear problem is modelled using two MILP sub-problems.

Therefore, calculating DC power flow at each step of the cascades is naturally a QCP problem until we apply this special transformation. To this end, we convert the original QCP problem of DC power flow in the presence of dynamic impedance to a relaxed Second-Order Cone Programming (SOCP) problem [22] and solve it efficiently using an interior point method. This transformation applies an exact relaxation that properly guarantees the accuracy of the obtained result.

Concerning the addition of DSR to the grids, the authors are not aware of any siting methodology for the devices that directly targets attenuation of cascading outage propagation. Therefore, in this paper, first, a new topological measure of proximity between branches within a power grid is proposed. Then the lines are clustered using this measure, and one line is selected from each cluster to install the DSR modules. It should be noted that our suggested methodology to add DSR to a power grid is notional and not intended to be optimal or definitive: rather it simply seeks to install DSR units in a credible and even spread across the lines in a power system.

The major contributions of the present paper are summarised as follows: the most important contribution is to investigate the intuition of applying an available and affordable FACTS device i.e., DSR, to arrest cascading line outages. Currently, DSR devices have different roles within the grid and their capabilities of mitigating cascading line outages have not been clearly evaluated in the literature. Second, we propose a novel methodology to solve DC power flow in the presence of dynamic impedance based on an exact relaxed Second-Order Cone Programming (SOCP) model which can be efficiently solved using an interior point method. The approximations considered for the normal DC power flow suffice to solve this novel DC-PF and it does not rely on any pre-solve simulations. Finally, a novel line-oriented topological measure is suggested which is able to reveal how meshed each pair of lines within the grid are. Furthermore, using this novel metric, the radial lines can be easily detected. This novel metric is then used to place DSR modules across the network.

The remainder of this paper is organised as follows. In Section II, the novel methodology for modelling DC-PF with dynamic impedances and the novel topological index is presented. In Sections III the test platform and various sample networks are described, and Section IV discussed the simulation results and various sensitivity analyses. Section V concludes.

II. Methodology

In this section, first, a novel DC-PF in the presence of DSR devices is formulated. Then, a new electrical distance for the branches within power grids termed *Lines Mesh Matrix* is proposed and used to place DSR devices within the grids. With these in hand, it is investigated how effective DSR are at arresting the cascading line outages.

DSR can either work autonomously or be controlled by a central operator. In this paper, we focus on their autonomous mode, as cascading failures often propagate rapidly and the control room may not be able to operate the devices fast enough. In the autonomous mode, the devices react instantly to change in the power flow they measure.

A. Modelling of DSR devices in load flow calculations

In this section, the proposed methodology to tailor DC-PF to include DSR devices is discussed. Consider a grid with N buses and L lines where $L_D \subset L$ is the sub-set of the lines with DSR modules installed. The DC-PF assumptions determine the active power flow for branch $L_{ij} \in L$ and $\forall i, j \in N$ as below:

$$p_{ij} = \frac{\delta_i - \delta_j}{X_{ij}} \tag{1}$$

Where X_{ij} and δ_i are the reactance of line L_{ij} and the voltage angle of bus i, respectively. If branch $L_{ij} \in L_D$, then Equation 1 is rewritten as follows:

$$p_{ij}.x_{ij}^{'} = \delta_i - \delta_j \tag{2}$$

Where,

$$x_{ij}^{'} = X_{ij}^{0} + x_{d,ij} \tag{3}$$

Where X_{ij}^{0} and $x_{d,ij}$ are the original natural reactance of L_{ij} and the imposed extra reactance to L_{ij}, respectively, and $x_{ij}^{'}$ is the new total reactance of L_{ij}. Based on the idealised control strategy presented in [2], the autonomous control scheme of the DSR installed on the branches, which involves five control zones, can be found in Fig. 2. To avoid adding more non-linearality to the programming model by considering absolute values of the flows, we consider the directions of the flows which results in expanding this scheme over both positive and negative amounts of active power flow: p_{ij} is positive if power goes from node i to node j. As discussed in [2], for a specific interval of active power flow, here determined by $[+\alpha, +\beta]$ for positive power and $[-\alpha, -\beta]$ for negative power, the DSR modules come online one by one and consequently, the imposed impedance increases step by step until it reaches its maximum amount. It is argued in [2] practically the activation interval should be set wide enough to allow all modules to come online. In the proposed method, this step by step increase is approximated by a straight line as can be seen in Fig. 2. Therefore, $x_{d,ij}$ is set as follows:

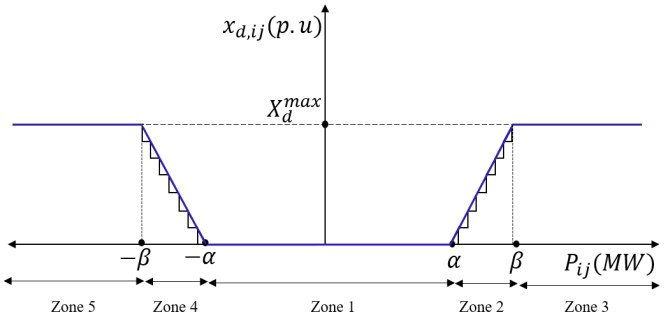

Fig. 2. DSR control zones

$$x_{d,ij} = \begin{cases} 0 & if \quad -\alpha \leq p_{ij} \leq +\alpha \\ \frac{X_d^{max}}{\beta-\alpha}.(p_{ij}-\alpha) & if \quad +\alpha \leq p_{ij} \leq +\beta \\ X_d^{max} & if \quad +\beta \leq p_{ij} \\ \frac{-X_d^{max}}{\beta-\alpha}.(p_{ij}+\alpha) & if \quad -\beta \leq p_{ij} \leq -\alpha \\ X_d^{max} & if \quad p_{ij} \leq -\beta \end{cases} \tag{4}$$

Where X_d^{max} is the maximum imposed impedance by DSR modules. The same as a normal DC-PF, in this adapted version the generation and demand levels are given as input parameters and are not optimised. The main differences between usual DC-PF and our proposed DC-PF are the new constraints presented in Equations 2 to 4 which turn the problem from a linear programme to a mixed integer non linear programme. Our novel methodology to tackle this major non-linearality is as follows:

Each control zone is represented by a binary variable like $u_{k,ij}$ so that the control zone k is activated iff $u_{k,ij} = 1$. Therefore, Equation 2 is rewritten as follow:

$$p_{ij}.[X_{ij}^0 u_{1,ij} + X_{ij}^0 u_{2,ij} + \frac{X_d^{max}}{\beta-\alpha}u_{2,ij}(p_{ij}-\alpha) + X_{ij}^0 u_{3,ij} + X_d^{max}u_{3,ij} + X_{ij}^0 u_{4,ij} - \frac{X_d^{max}}{\beta-\alpha}u_{4,ij}(p_{ij}+\alpha) + X_{ij}^0 u_{5,ij} + X_d^{max}u_{5,ij}] = \delta_i - \delta_j \tag{5}$$

Which can be rewritten as:

$$p_{ij}X_{ij}^0 u_{1,ij} + p_{ij}X_{ij}^0 u_{2,ij} + \frac{X_d^{max}}{\beta-\alpha}u_{2,ij}{p_{ij}}^2 - \frac{X_d^{max}}{\beta-\alpha}u_{2,ij}p_{ij}\alpha + p_{ij}X_{ij}^0 u_{3,ij} + p_{ij}X_d^{max}u_{3,ij} + p_{ij}X_{ij}^0 u_{4,ij} - \frac{X_d^{max}}{\beta-\alpha}u_{4,ij}{p_{ij}}^2 - \frac{X_d^{max}}{\beta-\alpha}u_{4,ij}p_{ij}\alpha + p_{ij}X_{ij}^0 u_{5,ij} + p_{ij}X_d^{max}u_{5,ij} = \delta_i - \delta_j \tag{6}$$

In Equation 6, we have two kinds of non-linear terms. The first type have a form like $p_{ij}u_{k,ij}$. These terms are substituted by another continuous variables, $\lambda_{k,ij}$, while the following linear constraints based on the *Big M* methodology [25] should be satisfied:

$$p_{ij} - (1-u_{k,ij})M_{ij} \leqslant \lambda_{k,ij} \tag{7}$$

$$\lambda_{k,ij} \leqslant p_{ij} + (1-u_{k,ij})M_{ij} \tag{8}$$

$$\lambda_{k,ij} \leqslant u_{k,ij}M_{ij} \tag{9}$$

$$\lambda_{k,ij} \geqslant -u_{k,ij}M_{ij} \tag{10}$$

$$M_{ij} \gg \eta_{ij}^{max} \tag{11}$$

Where M_{ij} is a big positive real number which is proportional to its corresponding line's loading capacity i.e., p_{ij}. Also, η_{ij}^{max} is the thermal loading limit of L_{ij}. The second type of the non-linearality are ${p_{ij}}^2 u_{k,ij}$. To tackle these non-linear terms, an exact relaxation is applied which turns the problem to a SOCP problem. To this end, first ${p_{ij}}^2$ is replaced using a new continuous variable, $\gamma_{k,ij}$, which produces another first type non-linear terms like $\gamma_{k,ij}u_{k,ij}$. These new first type non-linear terms are then replaced with new continuous variables, $\zeta_{k,ij}$, while the following linear constraints based on the *Big M* methodology should be satisfied:

$$\gamma_{k,ij} - (1-u_{k,ij})M'_{ij} \leqslant \zeta_{k,ij} \tag{12}$$

$$0 \leqslant \zeta_{k,ij} \leqslant u_{k,ij}\gamma_{k,ij} \tag{13}$$

$$\zeta_{k,ij} \leqslant u_{k,ij}M'_{ij} \tag{14}$$

$$M'_{ij} \gg (\eta_{ij}^{max})^2 \tag{15}$$

Where M'_{ij} is a big positive real number which is proportional to the square of its corresponding line's loading capacity i.e., ${p_{ij}}^2$. It should be noted that in our novel formulation, *Big M*s i.e., M_{ij} and M'_{ij}, are set for the lines with DSRs individually so that each line with DSR units has its specific sets of M_{ij} and M'_{ij}. This helps to tighten the optimization problem significantly and prevent numerical issues when solving the problem which results in a reasonably fast optimization.

The main non-linear constraint of this formulation which is still remaining is ${p_{ij}}^2 = \gamma_{k,ij}$, which can be written as an inequality as follows:

$${p_{ij}}^2 \leqslant \gamma_{k,ij} \tag{16}$$

Where $\gamma_{k,ij}$ is another continuous variable. As the problem is a constraint programming problem, the objective function is flexible and can be set with desirable characteristics. Accordingly, we propose an objective function that minimises the summation of all $\gamma_{k,ij}$, as can be seen in Equation 17. Note that the minimum of the objective function is achieved if $\gamma_{k,ij}$ is exactly set to ${p_{ij}}^2$. In this way the non-convex part of the problem is removed and an exact relaxation is applied for the

constraint presented in Equation 16 which gives the problem a SOCP configuration. Therefore, the problem of DC-PF in the presence of DSR modules can modelled as follows:

$$\textit{Objective function} = min(\sum_{L_{ij} \in L_D} \gamma_{k,ij}) \tag{17}$$

S.t.:

(6) to (16), and

$$p_{ij} + \beta \leqslant M_{ij}(u_{1,ij} + u_{2,ij} + u_{3,ij} + u_{4,ij}) \tag{18}$$

$$p_{ij} + \alpha \leqslant M_{ij}(u_{1,ij} + u_{2,ij} + u_{3,ij}) \tag{19}$$

$$p_{ij} - \alpha \leqslant M_{ij}(u_{2,ij} + u_{3,ij}) \tag{20}$$

$$p_{ij} - \beta \leqslant M_{ij}(u_{3,ij}) \tag{21}$$

$$-p_{ij} - \beta \leqslant M_{ij}(u_{5,ij}) \tag{22}$$

$$-p_{ij} - \alpha \leqslant M_{ij}(u_{4,ij} + u_{5,ij}) \tag{23}$$

$$-p_{ij} + \alpha \leqslant M_{ij}(u_{1,ij} + u_{4,ij} + u_{5,ij}) \tag{24}$$

$$-p_{ij} + \beta \leqslant M_{ij}(u_{1,ij} + u_{2,ij} + u_{4,ij} + u_{5,ij}) \tag{25}$$

$$\sum(u_{1,ij} + u_{2,ij} + u_{3,ij} + u_{4,ij} + u_{5,ij}) = 1 \tag{26}$$

The linear constraints presented in Equations 18 to 26 detect which control zone is activated.

B. Contingency analysis and simulation of cascading failures

To trigger possible cascading outages within power grids, first, some lines need to be removed as triggering events. In this paper, the predetermined number of most loaded branches, F, are removed from the grid as the triggering events of cascading outages, and then, the progression of subsequent outages, if any, are simulated. To detect the most loaded lines for the grid under a particular operational snapshot, a normal DC-PF is calculated.

To simulate the cascading failures caused by each triggering lines outage, a practical and simple algorithm is applied. The algorithm is based on DC-PF. At each step of the cascading outages, overloaded branches are tripped off and in the resulting islands, if any, the load-generation balance is kept by either shedding loads or adjusting the generation level [21]. This procedure continues until no overloaded line can be found within the grid.

C. Test system preparation

This section describes a procedure for augmenting power systems with DSR units, as such power flow devices are generally absent from standard test networks. The procedure described here is not intended to be optimal or definitive: rather it simply seeks to install DSR units in an even spread across the lines in a power system. As cascade propagation can be a global rather than a localised phenomenon, one may anticipate that DSR units will need to be distributed throughout the network to be effective at arresting cascades. For this reason, the present procedures introduce a new notion of electrical distance to ensure a wide and even dispersal of DSR units throughout the network. Various other legitimate siting methodology could likewise be proposed.

1) Lines Mesh Matrix: In this section, a new topological index for the branches within power grids termed as *Lines Mesh Matrix*, Π, is defined which relies on *Power Transfer Distribution Factor*, Φ, [26]. The proposed index investigates how lines contribute to handling specific transmissions of active power within the grid, to bring to light how mutually meshed the lines are with each other.

The dimension of Φ for a grid with n_l lines and n_b buses is $(n_l \times n_b)$ [26]. For a reference node like n_r, the column n_i of Φ shows the incremental power flow for each line in the grid for an injection at bus n_r and withdrawal at bus n_i. To build the Π matrix, a line within the grid like L_{ij} is considered and the contributions of all lines of the grid (including L_{ij}) for a unit active injection active power at the line's sending bus i and withdrawal at its receiving bus j are calculated. In a loose sense, this records how much redundant meshing there is, or how many alternative paths exist in parallel with L_{ij}. This procedure is repeated for all lines within the grid. Then, for each pair of lines within the grid like L_{ij} and L_{st}, the contributions of each of them for the injection and withdrawal of unit active power at either sides of the other one are compared together and the biggest value is selected as an index to show how *mutually meshed* these two lines are. Therefore, Π is a $(n_l \times n_l)$ matrix so that each row shows the results for its corresponding line. For line L_{ij}, its corresponding row, ℓ, is initialised as follows:

$$\begin{aligned} &\Pi(\ell\ ,\ :) = \Phi(:\ ,\ j) \\ &\text{S.t.:} \\ &\quad n_r = i, \quad P_i = 1, \quad P_j = -1 \end{aligned} \tag{27}$$

Then, in the Π matrix, $\forall m, n \in N$ and $m \neq n$, if $\Pi(n,\ m) \leq \Pi(m,\ n)$, $\Pi(n,\ m)$ is replaced with $\Pi(m,\ n)$. From Equation 27, one can notice that each diagonal component of Π shows the portion of power that is carried by the line itself when the injection of unit active power at one side of the line and withdrawal at the other side. Consequently, these diagonal components are equal to 1 for purely radial lines. Based on this important fact, the diagonal components can be considered as a *radiality index* for the lines:

$$\begin{aligned} &\mathfrak{R}_{ij} = \Pi(\ell\ ,\ \ell) \\ &0 \leqslant \mathfrak{R}_{ij} \leqslant 1 \end{aligned} \tag{28}$$

The idea of *radiality index* is reminiscent of the concept of *shortcut edges* [27] for graph geodesics.

Analysing the non-diagonal components within Π reveals how *mutually meshed* each pair of lines are within the grid so that the greater value of a non-diagonal component, the more tightly meshed a pair of corresponding lines are: they would seem likely to participate in the same bulk power transactions.

2) Notional procedure for adding DSR units to test networks: In this section, a novel method based on the Π matrix is suggested to locate DSR modules within the grid. As mentioned, the non-diagonal components in Π reflect how mutually meshed each pair of lines are within the grid. Therefore, applying a higher level clustering technique for the data available within Π enables us to detect the sub-groups of lines which are closely meshed together. Hence, the proposed placement methodology is based on clustering the branches into a certain number of groups using the data extracted from Π. After clustering the branches, for each group, one branch is selected as the chosen site for the installation of DSR modules.

As DSR units on radial lines are not able to change the lines' loading, at the first step, the radial lines are detected using the *radiality index* and then excluded from the possible lines to install the modules. To this end, the corresponding rows and columns of radial lines within Π are removed. To cluster the remaining branches using the reduced Π, $\Pi^{'}$, the dissimilarity matrix [28] needs to be obtained for $\Pi^{'}$. The dissimilarity matrix (D) for $\Pi^{'}$ is calculated as follow:

$$\mathrm{D} = \mathrm{I} - \Pi^{'} \tag{29}$$

Where I is the *all-ones matrix* [28]: this subtraction ensures that tightly meshed lines will have low dissimilarity to each other. Then, the diagonal components in D are artificially set to zero, and it is a symmetric and square matrix. Accordingly, the *K-medoids* clustering algorithm [29] is applied to the D matrix. This algorithm finds k centres, termed *medoids*, and clusters the components around these centres. For each cluster, a center (mediod) is one of the constituent components whose average dissimilarity to all other points in the cluster is minimal .Here, each line, represented by a row in D, is considered as a component for the *K-medoids* clustering algorithm so that the branches are clustered into a certain number of groups (here k groups) and the centre (medoid) of each cluster is selected as the place to install a module. Intuitively, when a selected line for installing DSR modules becomes overloaded, the modules act to reduce the line's power flow and shift it to the other adjacent lines (likely within the corresponding cluster) by imposing extra impedance onto the line.

The only aim of finding these clusters is to locate the DSR units across the network and no other functions are considered for the determined clusters.

III. Test platform

From the repository at [30], 8 sample grids are selected for this study. Firstly, for each test platform, all parallel lines are merged and replaced with an equivalent line. Then, for each of the grids 50 distinctive operational snapshots are leveraged from [31] which allows us to investigate the proposed methodologies across a wide range of grids, with each in a range of load and generator dispatch conditions. Here, an operational snapshot for a power system is considered as a specific load and generator dispatch condition for the grid.

For all the grids, each snapshot is evaluated with and without applying DSR modules by trying to initiate a cascade by considering ($F = 3$) [32]. Three distinctive penetration ratios, ∂, for DSR modules are considered under each snapshot. The penetration ratio is defined as the percentage of the lines with installed DSR modules within the grid. The three simulated penetration ratios are 5%, 10% and 25%. Therefore, the database includes 1600 different operational states which is a result of the sum of 400 different operation states without applying DSR units and the product of 8 sample grids, 50 different operational snapshots, and 3 different penetration ratios.

A. Implementing the methodology

To implement the methodology presented in this paper, three tool-boxes in MATLAB [33] are used. Test system data handling and augmentation uses the MATPOWER [34] tool-box. The novel DC-PF presented in Section II-A is modelled using YALMIP [35]. The cascading line outages are simulated using the MATCASC tool-box [21]. MATCASC implements the simple but effective algorithm explained in Section II-B to simulate the cascading line outages. The applicability of MATCASC was shown in [21] and also, verified later in [16]. In this paper, MATCASC uses the specific $(N-3)$ contingency mentioned in Section II-B as the triggering events. The original DC-PF component of MATCASC which is used to simulate the cascading failures is replaced with a new DC-PF script created using the methodology proposed in Section II-A to calculate line flows in the presence of DSR devices. Therefore, whenever MATCASC needs to run DC-PF during simulating the cascading failures, the new script is run instead of the original.

All of the scrips created to simulate the proposed methodologies of this paper and their related raw data can be found in [36].

B. DSR specifications

By installing several DSR modules on a line, greater total imposed impedance can be achieved [2]. Here, we assume the DSR modules can increase the impedance of their corresponding lines by an additional 40% above the original impedance. This proportional increase assumption aligns with [3], [23]. Also, for simplicity, all branches in a system, including transformers, are considered as potential sites for DSR modules: the implementation aspects of such installations are considered beyond the scope of the present work. Lastly, it is assumed that the DSR units are activated if the line's loading goes beyond 80% of its thermal loading limit and beyond 100%, the maximum capacity of the DSR is imposed. The DSR specifications presented in Fig. 2 are set as follows: $\alpha = 0.8\eta_{ij}^{max}$, $\beta = \eta_{ij}^{max}$, $X_D^{max} = 0.4X_{ij}^0$.

At each step of the cascading failures, if any lines with DSR installed on turns to a radial line after updating the topology of the grid, the DSR is deactivated. *Radiality index* presented in Section II-C1 is used to detect the radial lines.

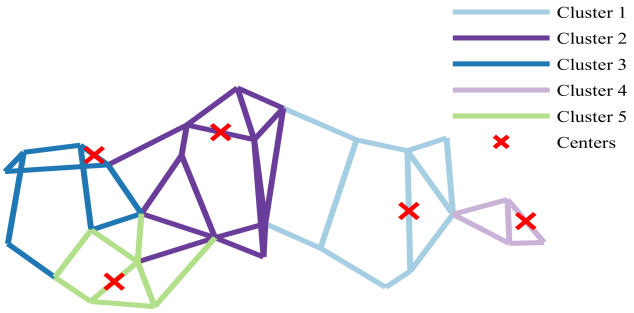

Fig. 3. A sample clustering scheme for `nesta_case29_ieee` with $\partial = 10\%$

TABLE I.
THE EFFECTS OF DSR PENETRATION ON THE AVERAGE LOAD-SHEDDING FOR THE CLUSTERING METHODOLOGY

Sample grid	Average load shed	Differential		
	$\partial = 0\%$	$\partial = 5\%$	$\partial = 10\%$	$\partial = 25\%$
`nesta_case29_ieee`	11.68 %	+2.21 pp	-0.04 pp	-2.63 pp
`nesta_case30_as`	2.46 %	-0.27 pp	-0.27 pp	+0.65 pp
`nesta_case30_ieee`	7.1 %	0 pp	0 pp	-0.56 pp
`nesta_case39_ieee`	11.85 %	0 pp	-0.01 pp	+0.21 pp
`nesta_case57_ieee`	12.25 %	0 pp	+0.04 pp	0 pp
`nesta_case73_ieee_rts`	7.26 %	-0.47 pp	+0.3 pp	-0.29 pp
`nesta_case118_ieee`	8.45 %	-0.72 pp	+0.99 pp	-0.87 pp
`nesta_case189_ieee`	31.46 %	0 pp	-1.9 pp	0 pp

IV. RESULTS

A. Simulation results

At the first step, the clustering technique proposed in Section II-C2 is applied to all sample grids to identify suitable sites for the DSR modules. In Fig. 3, as an example, the result obtained from the clustering methodology for `nesta_case29_ieee` under $\partial = 10\%$ can be seen, visualised using the methodology presented in [37]. Due to space shortage, the clusters found by the methodology for all sample grids are not presented here and instead, can be found in [36].

After locating DSR modules within all networks, the effects of the modules on cascade propogation are investigated. For each snapshot, first, as a base case, it is assumed that no DSR is installed within the grid, and then it is assumed that the DSR units are installed on the predetermined lines. The three most heavily loaded lines are removed in each snapshot in at attempt to provoke a cascading outage and the obtained results are compared. It should be noted that if removing the first 3 lines does not lead to any further removals, the obtained results are excluded from the simulation results.

The final load shedding percentages in the unaugmented grids, averaged over all operational snapshots where cascades occurred, are shown in the first column of Table I. The three rightmost columns then show the effect of adding DSR in different penetration ratios, recording the *percentage point* change in the average load shedding. In this table, the *improvement* and *disimprovement* and *no change* are colored with green, red, and grey, respectively, and *pp* denotes *percentage point*. Here *improvement* means less load-shedding . Counting the green cells in this table shows that in 11 out of 24 scenarios the DSR units have mitigated the cascading failures' average damage. In 6 conditions they have made the conditions worse and in 7 conditions they haven't had any effects on the average load-shedding.

While this table shows that in some cases the devices can be helpful to mitigate the load-shedding caused by the cascades, in general the changes are not very significant, neither in the improvements nor in the disimprovements. It seems that the initial intuition about the abilities of DSR to mitigate the consequences of the cascading outages has been mistaken. Of course, these data are averages and a small figure could obscure underlying variance.

At the next step, we need to further explore the details of the devices' underwhelming effects on the cascading failures. To this end, in Fig. 4 the obtained results for each grid under all operational snapshots where cascades occurred are available for three metrics of cascade severity: the total number of removed lines (a), the cascades' steps count (b) and the final amount of load-shedding (c). Each point in each scatterplot pane encodes an operational snapshot, with its horizontal ordinate denoting baseline performance, and vertical ordinate the post-augmentation condition. It should be noted that two metrics, removed lines count (a) and load-shedding (c), represent tangible damage to the grid, whereas cascades' steps count (b) is a more abstract measure of cascade propogation depth.

From Fig. 4 one can immediately notice that across many snapshots the devices have had minimal on no effects on the cascading failures: most points in most panes lie on the identity line diagonal. This finding was anticipated by Table I. However, in a few conditions, significant improvements can be noted. For example, in Fig. 4 (c) `nesta_case29_ieee` and `nesta_73_ieee_rts` with $\partial = 25\%$, there are some situations where after the first outages, the cascades stopped immediately and no further removals and load-shedding were detected. For the same operational snapshots without DSR units notable load-shedding and removals occur. On the other hand, in a few conditions one may also detect some significant disimprovements. For example, in `nesta_case29_ieee` with $\partial = 25\%$ and `nesta_118_ieee` with $\partial = 5\%$ notable disimprovement for the operational snapshots are apparent. Thus, no specific consequences in terms of the damages can be expected for applying the models.

Fig. 4 also shows `nesta_case189_ieee` is quite vulnerable against the attacks. This could be due to the topology of the grid, as it includes only a few non-radial lines. The average of the radiality index for all lines of this grid is reported 0.93, determining the structure is mainly radial. The attacks remove some of the important non-radial lines, resulting in severe damage to the grid.

From Table I and Fig. 4, in general, it seems that the devices have made no consistent mitigation of the cascading failures and this is in contrast with the initial intuition regarding their abilities to arrest the propagation of line overloads.

B. Sensitivity analysis

1) Sensitivity to DSR *locations:* As the obtained results in Section IV-A showed no major ability of the devices to arrest cascading outages, it is necessary to verify if the underwhelming performance is the fault of our placement methodology. In this section, a more direct methodology, using the empirical

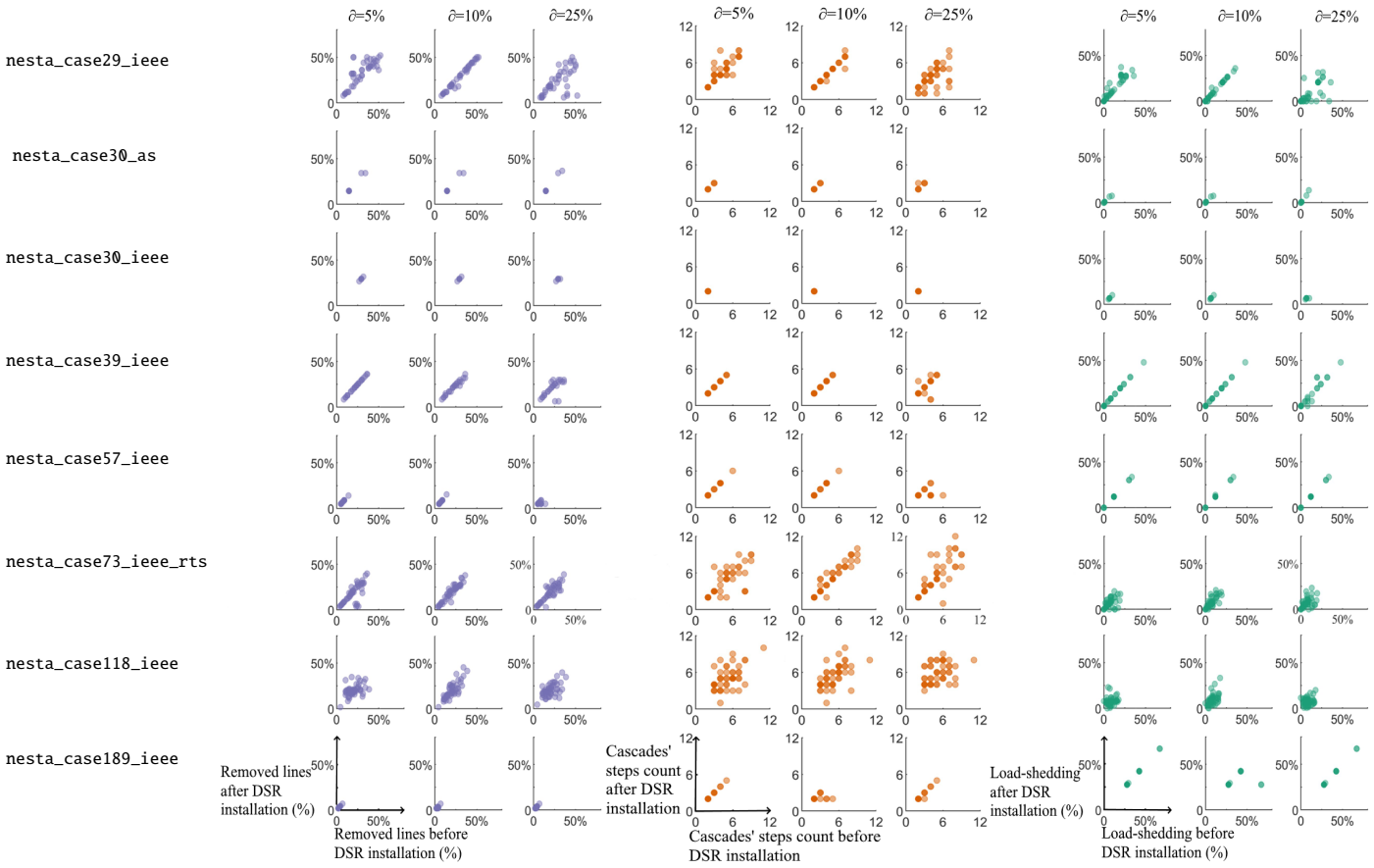

(a) Line removals (b) Cascades' steps count (c) Load-shedding

Fig. 4. The cascades' specifications comparison for the sample grids under different operational scenario

TABLE II.
THE PROPORTION OF ACTIVATED DSR FOR THE CLUSTERING METHODOLOGY, AVERAGED ACROSS ALL STAGES OF ALL CASCADES

Sample grid	∂ = 5%	∂ = 10%	∂ = 25%
nesta_case29_ieee	5.54%	7.72%	10.79%
nesta_case30_as	0.25%	0.53%	1.66%
nesta_case30_ieee	0%	6%	0.67%
nesta_case39_ieee	0%	2.02%	4.68%
nesta_case57_ieee	0%	0.86%	1.91%
nesta_case73_ieee_rts	8.34%	5.13%	3.12%
nesta_case118_ieee	20.55%	16.59%	8.2%
nesta_case189_ieee	0.5%	2.49%	2.66%

TABLE III.
THE PROPORTION OF ACTIVATED DSR FOR THE EMPIRICAL METHODOLOGY, AVERAGED ACROSS ALL STAGES OF ALL CASCADES

Sample grid	∂ = 5%	∂ = 10%	∂ = 25%
nesta_case29_ieee	25.68%	19.34%	16.06%
nesta_case30_as	2.58%	4.83%	4.72%
nesta_case30_ieee	6%	3%	3.82%
nesta_case39_ieee	19.02%	18.45%	9.27%
nesta_case57_ieee	2%	3.91%	5.19%
nesta_case73_ieee_rts	12.02%	15.17%	11.15%
nesta_case118_ieee	45.98%	40.91%	33.98%
nesta_case189_ieee	5.56%	3.25%	9.74%

cascading simulation data, is applied, to see if explicitly targeting DSR units onto lines known to be vulnerable can enhance their efficacy. The goal of this *empirical* placement methodology is to achieve more activation of DSR units during the cascades. From the simulations in Section IV-A, the lines that were most frequently outaged during cascading failures (before applying any DSR modules) are directly identified. After excluding the radial lines from the identified lines, as an attempt to achieve more activation of DSR units during the cascades, the devices are installed on these most frequently removed lines. For instance, for ∂ = 5%, the modules are installed on the top 5% of the most frequently removed lines and so on.

In Tables II and III, the averages of DSR module activation counts during the cascades are presented and visualised for the *clustering methodology* and the *empirical methodology*, respectively. For instance, the top left element of Table II tells us that in a typical stage of a typical cascade for nesta_case29_ieee just 5.54% of the available DSR units were activated. For both tables, darker blue infills denote greater values. From these two tables, one can immediately note that the *empirical methodology* increases the chance of the engagement for DSR significantly in comparison with it for the *clustering methodology* and therefore, the main purpose of the *empirical methodology* is achieved. The generally low values in Table. II might suggest that the underwhelming performance seen in Section IV-A may stem from poorly sited DSR units failing to

activate.

To explore this further, the percentage point differential between the average of load-shedding before and after applying the devices for the *empirical methodology* can be found in Table IV. These results show that, even with a much greater level of DSR activation, the effect on actual load shedding is still slight, and the empirical siting methodology fails to majorly improve on the earlier underwhelming results in Table I. The situation for `nesta_case39_ieee` has somewhat improved, and `nesta_case29_ieee` disimproved, with null or modest gains evident for other systems.

2) Sensitivity to DSR *parameters:* In this section, the sensitivity to the DSR parameters of the model presented in Fig. 2 is investigated for the obtained results . To this end, a new set of parameters are chosen: $\alpha = 0.65\eta_{ij}^{max}$, $\beta = 0.9\eta_{ij}^{max}$, $X_D^{max} = 0.35X_{ij}^0$.

The results in Table. V further indicate that our initial intuition regarding the abilities of the DSR devices to arrest cascading outages was wrong. This finding was also understood before from the results in Table. I.

3) Sensitivity to the contingency type: This section provides a further sensitivity analysis, by varying the type of triggering contingency event. To this end, we simulate two additional types of branch outage events for the full range of DSR penetration levels across the 50 operational snapshots on the 8 test grids. The DSR locations and parameters are per the initial clustering siting methodology.

Firstly, we repeat the previous maximum loading branch removal strategy but with ($F = 2$) rather than = 3, so that the *two* lines with the highest MW flow are removed for each snapshot of a particular grid. Removing a different number of lines results in an altered topology for the grid after the triggering attack and consequently affects the overall trajectory of the cascades' propagation. In this way, the efficacy of the modules is further investigated with a different sampling of potential cascade propagation pathways. The obtained summary results for this new type of contingency can be found in Table. VI. This table shows the modules are still not significantly effective at arresting the cascades and further implies that our initial intuition was not correct.

Next, we investigate if the homogeneous results are due to the maximum loading based attack strategy chosen to trigger the cascades. To this end, we carry out a new attack strategy based on *random* removal of three lines ($F = 3$). However, as shown in [32], purely random attacks are not usually damaging enough to trigger a cascade. To address this issue, after randomly selecting three lines to be removed, we first check to see if these lines' removals triggers a cascade for the corresponding snapshot in the baseline grid without DSR units installed. If not, another three random lines are selected and this procedure continues until we identify a set of three lines for every snapshot of every grids whose removal is an initialising event with the ability to trigger a cascade. These randomised removal attacks allow a broad range of branches to be involved in the initialising contingency for the cascade simulations. The efficacy of the DSR to arrest the cascades with this new attack strategy is then investigated and presented in Table. VII. Once again, the results of this table reveal, as with the previously obtained results, that the modules do not show a promising ability to arrest cascading failures.

TABLE IV.
THE EFFECTS OF DSR PENETRATION ON THE AVERAGE LOAD-SHEDDING FOR THE EMPIRICAL METHODOLOGY

Sample grid	Average load shed	Differential		
	∂ = 0%	∂ = 5%	∂ = 10%	∂ = 25%
`nesta_case29_ieee`	11.68 %	+2.58 pp	+3.1 pp	+1.14 pp
`nesta_case30_as`	2.46 %	0 pp	0 pp	+0.27 pp
`nesta_case30_ieee`	7.1 %	0 pp	0 pp	+3 pp
`nesta_case39_ieee`	11.85 %	-2.7 pp	-5 pp	-5.2 pp
`nesta_case57_ieee`	12.25 %	0 pp	0 pp	-0.09 pp
`nesta_case73_ieee_rts`	7.26 %	-0.4 pp	-3.1 pp	-3.3 pp
`nesta_case118_ieee`	8.45 %	-1.7 pp	-3.1 pp	-2.6 pp
`nesta_case189_ieee`	31.46 %	-0.96 pp	-0.96 pp	-0.96 pp

TABLE V.
THE EFFECTS OF DSR PENETRATION ON THE AVERAGE LOAD-SHEDDING FOR THE CLUSTERING METHODOLOGY WITH DIFFERENT SET OF CONTROLLING PARAMETERS

Sample grid	Average load shed	Differential		
	∂ = 0%	∂ = 5%	∂ = 10%	∂ = 25%
`nesta_case29_ieee`	11.68 %	+3.32pp	+0.35 pp	-1.76 pp
`nesta_case30_as`	2.46 %	-0.26 pp	-0.26 pp	+0.15 pp
`nesta_case30_ieee`	7.1 %	0 pp	0 pp	-0.56 pp
`nesta_case39_ieee`	11.85 %	0 pp	0 pp	+0.52 pp
`nesta_case57_ieee`	12.25 %	0 pp	+0.04 pp	0 pp
`nesta_case73_ieee_rts`	7.26 %	-0.15 pp	-0.67 pp	-1.06 pp
`nesta_case118_ieee`	8.45 %	+2.4pp	+2.4 pp	+0.3 pp
`nesta_case189_ieee`	31.46 %	+0.96 pp	0 pp	+0.96 pp

C. Analysing the obtained data

This section presents some deeper analysis of the obtained baseline data in section IV-A. First of all, arresting the propagation by DSR modules does not necessarily lead to less damage to the grid. For example, in Fig. 4 for `nesta_case57_ieee` with $\partial = 25\%$, while after applying the modules the grid experiences fewer outages and cascades, the damage to the grid does not change. This is because the modules fail to prevent the major outage(s) causing the damage. This important insight implies that saving some lines by the modules during the cascades may not be sufficient to mitigate the overall resulting damages.

Another important point is that applying DSR units may change the pattern of the cascades propagation in comparison with what it was for the original grid. The modules may push back the power from their corresponding lines and redistribute it onto other lines within the grid. The redistributed power could stress the affected lines, resulting in changing the propagation and its consequences. This fact implies that the propagation of the cascades before and after applying the modules may involve non-overlapping sets of lines. If the DSR saves at least one line, the number of overlapping lines before and after applying the modules will decrease. The uncertain consequences for the grids in terms of the damages, either load-shedding or removed lines, derives from the changes within these patterns. For example, for `nesta_case118_ieee` with $\partial = 25\%$, there is a condition where applying the modules changes the propagation pattern so that 91% of the removed lines overlap with the removed lines in the cascades within the original grid. In this specific condition, the load-shedding drops from 15.79% before applying the modules to 5.52% after applying the DSR. Fig. 5(a) shows this comparison. For the same grid and ∂, there is a situation where after applying the modules, the propagation

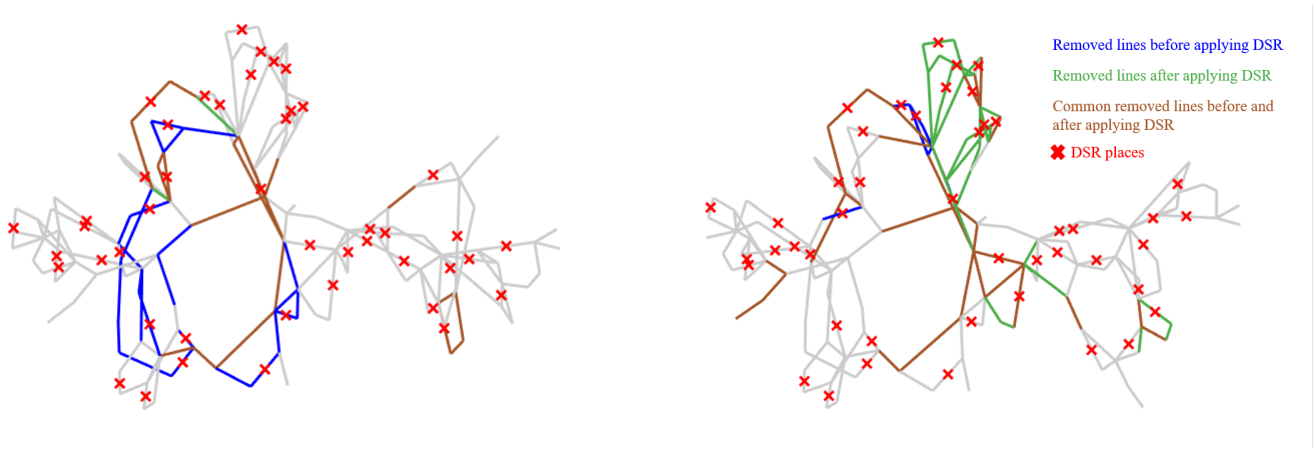

(a) DSR change the propagation, resulting in less load-shedding

(b) DSR change the propagation, resulting in more load-shedding

Fig. 5. Cascades's propagation comparison for `nesta_case118_ieee` under two particular operational snapshots with $\partial = 25\%$ before and after applying DSR, the DSR located using the clustering methodology.

TABLE VI.
THE EFFECTS OF DSR PENETRATION ON THE AVERAGE LOAD-SHEDDING FOR THE CLUSTERING METHODOLOGY ($F = 2$)

Sample grid	Average load shed	Differential		
	$\partial = 0\%$	$\partial = 5\%$	$\partial = 10\%$	$\partial = 25\%$
`nesta_case29_ieee`	8.88 %	+3.56pp	+0.26 pp	+0.05 pp
`nesta_case30_as`	6.39 %	+0.58 pp	+0.58 pp	+0.19 pp
`nesta_case30_ieee`	0.85 %	0 pp	0 pp	0 pp
`nesta_case39_ieee`	19.04 %	0 pp	-0.28 pp	-1.94 pp
`nesta_case57_ieee`	11.07 %	0 pp	0 pp	0pp
`nesta_case73_ieee_rts`	5.32 %	-0.64 pp	-0.24 pp	-2.01 pp
`nesta_case118_ieee`	9.29 %	-1.42pp	+0.4 pp	-2.22 pp
`nesta_case189_ieee`	27.71 %	0 pp	0 pp	0 pp

TABLE VII.
THE EFFECTS OF DSR PENETRATION ON THE AVERAGE LOAD-SHEDDING FOR THE CLUSTERING METHODOLOGY, APPLYING THE NEW RANDOM ATTACK STRATEGY

Sample grid	Average load shed	Differential		
	$\partial = 0\%$	$\partial = 5\%$	$\partial = 10\%$	$\partial = 25\%$
`nesta_case29_ieee`	2.93 %	+0.57pp	-0.08pp	-1.11 pp
`nesta_case30_as`	11.85 %	0 pp	0 pp	+0.33 pp
`nesta_case30_ieee`	1.79 %	0 pp	0 pp	-0.18 pp
`nesta_case39_ieee`	7.21 %	0 pp	-0.55 pp	-0.01 pp
`nesta_case57_ieee`	5.31 %	0 pp	+0.19 pp	-1.23 pp
`nesta_case73_ieee_rts`	1.5 %	+0.23 pp	-0.23 pp	-0.08 pp
`nesta_case118_ieee`	6.12 %	-2.68pp	-2.61 pp	-1.89 pp
`nesta_case189_ieee`	2.81 %	0 pp	0 pp	0 pp

changes so that 49% of the removed lines overlap with the removed lines in the cascades propagation for the original grid. In this specific condition, changing the propagation pattern increases the load-shedding from 3.98% within the original grid for the same contingency to 20.89%. Fig. 5(b) shows this comparison. Thus, changing the pattern of the propagation due to the DSR effects results in uncertain consequences in terms of the damage.

Furthermore, from Table. III, the greatest activation averages are reported for `nesta_case118_ieee` and `nesta_case29_ieee`, respectively. The corresponding results of these two sample grids in Table. IV show while significant improvements in load-shedding are reported for `nesta_case118_ieee` under all values of ∂ , sever disimprovements in load-shedding for `nesta_case29_ieee` under all values of ∂ can be seen. This important fact, firstly, entails obtaining more activated modules by applying different installation methodologies does not necessarily result in mitigating the cascading outages, and secondly, can be another prove for the uncertain consequences following the changes in the propagation pattern after DSR applications.

All of these remarkable findings reveal the DSR devices show no promising abilities to arrest the cascading line outages.

D. Discussion

In this study, to evaluate the efficacy of the DSR units to arrest cascades, we evaluated the modules on 8 different grids, each of which under 50 distinctive operational snapshots. Then, we carried out three different sensitivity analyses for the obtained results, varying the modules' siting methodology, the DSR specifications and the contingency types. This broad-based investigation resulted in simulating 7200 distinct contingency events for the various grids. The results obtained from these comprehensive simulations showed that, unlike the initial intuition, DSR modules are not significantly effective at arresting the propagation of cascading failures in most situations.

While Fig. 2 illustrates an idealised situation where DSR units protect a network from cascading outages, the discouraging simulation results imply that, in practise, such protective effects only rarely arise.

Many factors may contribute to the underwhelming results. A very important point to consider is that the propagation of cascading outages within power systems is a non-linear phenomena so that removing lines from the grid may have very complicated effects on the other lines within the system [15], [38]. In cascading failures we are dealing with a chaotic phenomena and trying to intervene in a fractal type and chaotic phenomena is not intuitive. The results of this paper further support this important observation so that, despite the initial

intuition about the potential efficacy of DSR, the intervention through this specific kind of FACTS devices on cascading failures is found to not be significantly successful. While application of DSR in a targeted way may help with specific grid vulnerabilities, their generalised addition to a power system does not appear to reduce how 'brittle' a grid is.

Last but not least, although the efficacy of the DSR devices against cascading failures was not found to be successful, the devices stay quite beneficial in their regular applications such as maintenance purposes and improving the loadability of the grids.

V. Conclusion

In this paper, the ability of DSR modules to arrest the propagation of cascading failures within power grids was investigated. To this end, first, a new formulation for the DC power flow calculations in the presence of the DSR units was developed. In this novel formulation, an exact relaxation is applied to model the problem using a SOCP formulation. Then, a novel topological measure for power networks was suggested, and a clustering methodology was introduced, to place the devices evenly throughout the grids. The simulation results showed that, unlike the initial intuition, the devices are not significantly effective at arresting cascades in many cases. This conclusion was further verified by a sensitivity analysis for the DSR locations, which directly placed the DSR units on those lines observed to suffer the most overloading during cascades. Even with the advantage of such a 'retrospective' placement strategy, the efficacy of the DSR units remained underwhelming. This could be due to the changes within the pattern of the propagation after DSRs activation resulting in uncertain consequences. A further sensitivity analysis, which varied the type of the triggering contingency, likewise failed to reveal any meaningful protective role afforded by the presence of DSR modules. Cascading line outages are chaotic phenomena where any interventions to control the propagation may lead to unexpected consequences. This paper did not find compelling evidence that making a power system less 'brittle' by installing many DSR units is associated with less severe or less sudden cascading failure dynamics.

Acknowledgement

The authors would like to express their acknowledgment to Dr. Alireza Nouri (University College Dublin) and Dr. Alireza Soroudi (University College Dublin) for their kind supports to conduct this research.

References

[1] H. Nagarajan, E. Yamangil, R. Bent, P. Van Hentenryck, and S. Backhaus, "Optimal resilient transmission grid design," in *2016 Power Systems Computation Conference (PSCC)*, 2016, pp. 1–7.

[2] H. Johal, "Distributed series reactance: A new approach to realize grid power flow control," Ph.D. dissertation, Georgia Institute of Technology, Dec. 2008.

[3] M. Sahraei-Ardakani and K. W. Hedman, "A fast lp approach for enhanced utilization of variable impedance based facts devices," *IEEE Transactions on Power Systems*, vol. 31, no. 3, pp. 2204–2213, 2016.

[4] K. Rahimi, H. Jain, R. Broadwater, and J. Hambrick, "Application of distributed series reactors in voltage balancing," in *2015 IEEE Power Energy Society General Meeting*, 2015, pp. 1–5.

[5] K. Rahimi, H. Jain, and R. Broadwater, "Application of distributed series reactors in relieving congestion costs," in *2016 IEEE/PES Transmission and Distribution Conference and Exposition (T D)*, 2016, pp. 1–5.

[6] A. Onen, "Investigation of distributed series reactors in power system applications and its economic implementation," *International Transactions on Electrical Energy Systems*, vol. 27, no. 3, e2259, 2017, e2259 ETEP-15-0452.R2.

[7] D. Das, F. Kreikebaum, D. Divan, and F. Lambert, "Reducing transmission investment to meet renewable portfolio standards using smart wires," in *IEEE PES T D 2010*, 2010, pp. 1–7.

[8] A. Soroudi, P. Maghouli, and A. Keane, "Resiliency oriented integration of dsrs in transmission networks," *IET Generation, Transmission Distribution*, vol. 11, no. 8, pp. 2013–2022, 2017.

[9] X. Zhang, K. Tomsovic, and A. Dimitrovski, "Security constrained multi-stage transmission expansion planning considering a continuously variable series reactor," *IEEE Transactions on Power Systems*, vol. 32, no. 6, pp. 4442–4450, 2017.

[10] N. Ghadimi, "Probabilistic decomposition-based security constrained transmission expansion planning incorporating distributed series reactor," English, *IET Generation, Transmission & Distribution*, vol. 14, 3478–3487(9), 17 Sep. 2020.

[11] B. A. Carreras, D. E. Newman, I. Dobson, and A. B. Poole, "Evidence for self-organized criticality in a time series of electric power system blackouts," *IEEE Transactions on Circuits and Systems I: Regular Papers*, vol. 51, no. 9, pp. 1733–1740, 2004.

[12] D. P. Nedic, I. Dobson, D. S. Kirschen, B. A. Carreras, and V. E. Lynch, "Criticality in a cascading failure blackout model," *International Journal of Electrical Power & Energy Systems*, vol. 28, no. 9, pp. 627–633, 2006.

[13] B. A. Carreras, V. E. Lynch, I. Dobson, and D. E. Newman, "Critical points and transitions in an electric power transmission model for cascading failure blackouts," *Chaos: An Interdisciplinary Journal of Nonlinear Science*, vol. 12, no. 4, pp. 985–994, 2002.

[14] Y. Koç, M. Warnier, P. Van Mieghem, R. E. Kooij, and F. M. Brazier, "A topological investigation of phase transitions of cascading failures in power grids," *Physica A: Statistical Mechanics and its Applications*, vol. 415, pp. 273–284, 2014.

[15] P. D. H. Hines, I. Dobson, and P. Rezaei, "Cascading power outages propagate locally in an influence graph that is not the actual grid topology," *IEEE Transactions on Power Systems*, vol. 32, no. 2, pp. 958–967, 2017.

[16] A. Beiranvand and P. Cuffe, "A topological sorting approach to identify coherent cut-sets within power grids," *IEEE Transactions on Power Systems*, vol. 35, no. 1, pp. 721–730, 2020.

[17] L. Che, X. Liu, and Z. Shuai, "Optimal transmission overloads mitigation following disturbances in power systems," *IEEE Transactions on Industrial Informatics*, vol. 15, no. 5, pp. 2592–2604, 2019.

[18] S. Hosseinalipour, J. Mao, D. Y. Eun, and H. Dai, "Prevention and mitigation of catastrophic failures in demand-supply interdependent networks," *IEEE Transactions on Network Science and Engineering*, vol. 7, no. 3, pp. 1710–1723, 2020.

[19] C. Chen, W. Ju, K. Sun, and S. Ma, "Mitigation of cascading outages using a dynamic interaction graph-based optimal power flow model," *IEEE Access*, vol. 7, pp. 168 637–168 648, 2019.

[20] M. Koenig, P. Duggan, J. Wong, M. Y. Vaiman, M. M. Vaiman, and M. Povolotskiy, "Prevention of cascading outages in con edison's network," in *IEEE PES T D 2010*, 2010, pp. 1–7.

[21] Y. Koc, T. Verma, N. A. M. Araujo, and M. Warnier, "Matcasc: A tool to analyse cascading line outages in power grids," in *2013 IEEE International Workshop on Inteligent Energy Systems (IWIES)*, 2013, pp. 143–148.

[22] J. Lee and S. Leyffer, *Mixed Integer Nonlinear Programming*. Springer Publishing Company, Incorporated, 2011.

[23] Y. Sang and M. Sahraei-Ardakani, "Effective power flow control via distributed facts considering future uncertainties," *Electric Power Systems Research*, vol. 168, pp. 127–136, 2019.

[24] O. Ziaee, O. Alizadeh-Mousavi, and F. F. Choobineh, "Co-optimization of transmission expansion planning and tcsc placement considering the correlation between wind and demand scenarios," *IEEE Transactions on Power Systems*, vol. 33, no. 1, pp. 206–215, 2018.

[25] A. Nouri, S. H. Hosseini, and A. Keane, "Stochastic network constrained payment minimisation in electricity markets," English, *IET Generation, Transmission & Distribution*, vol. 13, 2268–2279(11), 11 Jun. 2019.

[26] R. D. Christie, B. F. Wollenberg, and I. Wangensteen, "Transmission management in the deregulated environment," *Proceedings of the IEEE*, vol. 88, no. 2, pp. 170–195, Feb. 2000.

[27] M. Papagelis, "Refining social graph connectivity via shortcut edge addition," *ACM Trans. Knowl. Discov. Data*, vol. 10, no. 2, Oct. 2015, ISSN: 1556-4681. DOI: 10.1145/2757281.

[28] I. Amerise and A. Tarsitano, "Combining dissimilarity matrices by using rank correlations.," *Computational Statistics*, vol. 31, no. 1, pp. 353–367, 2016.

[29] A. Struyf, M. Hubert, and P. Rousseeuw, "Clustering in an object-oriented environment," *Journal of Statistical Software, Articles*, vol. 1, no. 4, pp. 1–30, 1997.

[30] C. Coffrin, D. Gordon, and P. Scott, "NESTA: The nicta energy system test case archive," Sep. 2014.

[31] P. Cuffe, "Raw data from "A comparison of malicious interdiction strategies against electrical networks"," May 2017. DOI: 10.6084/m9.figshare.4970804.v1.

[32] P. Cuffe, "A comparison of malicious interdiction strategies against electrical networks," *IEEE Journal on Emerging and Selected Topics in Circuits and Systems*, vol. 7, no. 2, pp. 205–217, Jun. 2017.

[33] MATLAB, *version 7.10.0 (R2019a)*. Natick, Massachusetts: The MathWorks Inc., 2019.

[34] R. D. Zimmerman, C. E. Murillo-Sanchez, and R. J. Thomas, "MATPOWER: Steady-state operations, planning, and analysis tools for power systems research and education," *IEEE Transactions on Power Systems*, vol. 26, no. 1, pp. 12–19, Feb. 2011.

[35] J. Lofberg, "YALMIP : A toolbox for modeling and optimization in MATLAB," in *2004 IEEE International Conference on Robotics and Automation (IEEE Cat. No.04CH37508)*, Sep. 2004, pp. 284–289.

[36] A. Beiranvand and P. Cuffe, "Raw data and scripts from Negative Results on Deploying Distributed Series Reactance Devices to Improve Power System Robustness Against Cascading Failures," DOI: 10.6084/m9.figshare.12301685.

[37] P. Cuffe and A. Keane, "Visualizing the electrical structure of power systems," *IEEE Systems Journal*, vol. 11, no. 3, pp. 1810–1821, 2017.

[38] P. Crucitti, V. Latora, and M. Marchiori, "Model for cascading failures in complex networks," *Phys. Rev. E*, vol. 69, p. 045 104, 4 Apr. 2004.